Phys. Scr. **T129** (2007) 12–16 doi:10.1088/0031-8949/2007/T129/003

Local symmetry-reduction in tetragonal (La,Fe)-codoped $Pb[Zr_{0.4}Ti_{0.6}]O_3$ piezoelectric ceramics

Emre Erdem[1], Rüdiger-A Eichel[1], Hans Kungl[2], Michael J Hoffmann[2], Andrew Ozarowski[3], Hans van Tol[3] and Louis Claude Brunel[3]

[1] Eduard-Zintl-Institut, Technische Universität Darmstadt, D-64287 Darmstadt, Germany
[2] Institute of Ceramics in Mechanical Engineering, University of Karlsruhe, D-76131 Karlsruhe, Germany
[3] Center for Interdisciplinary Magnetic Resonance, National High Magnetic Field Laboratory, Florida State University, Tallahassee, FL 32310, USA

E-mail: eichel@chemie.tu-darmstadt.de

Received 31 March 2007
Accepted for publication 17 August 2007
Published 22 November 2007
Online at stacks.iop.org/PhysScr/T129/12

Abstract
Ferroelectric $Pb[Zr_{0.4}Ti_{0.6}]O_3$ ceramics codoped with La^{3+} and Fe^{3+} at dopant concentrations of 1.0 and 0.5 mol. %, respectively, were investigated by means of multifrequency electron paramagnetic resonance (EPR) spectroscopy. The results prove that iron is incorporated at the [Zr,Ti]-site, acts as an acceptor and favors the creation of charged $(Fe'_{Zr,Ti} - V_O^{\bullet\bullet})^{\bullet}$ defect dipoles that may give rise to *internal bias fields* also for '*soft*' piezoelectric compounds. In particular, the iron functional center site symmetry was investigated. A multi-site situation was observed in which the orientation of the $(Fe'_{Zr,Ti} - V_O^{\bullet\bullet})^{\bullet}$ defect dipole with respect to the orientation of spontaneous polarization is responsible for a $(Fe'_{Zr,Ti} - V_O^{\bullet\bullet})^{\bullet}$ center of 'tetragonal' and a different center of 'rhombic' local site symmetry.

PACS numbers: 61.72.Ji, 61.72.Bb, 85.50.−n

1. Introduction

Piezoelectric ceramics of the lead zirconate titanate solid solution system $Pb[Zr_xTi_{1-x}]O_3$, (PZT $x/1-x$) reveal excellent electromechanical properties [1]. For specific applications, device properties generally are tailored by doping with aliovalent transition-metal or rare-earth ions on a percentage level. Hence, there exists major interest in characterizing the exact role of the dopant ions as well as studying their immediate surroundings in order to develop microscopic models and to optimize device properties. As a *method-of-choice* for the study of such low-abundant functional centers, electron paramagnetic resonance (EPR) spectroscopy has proved to give valuable insights into the prevailing defect structure [2]. Macroscopically, it has been observed that acceptor-type Fe^{3+}-doping has a pronounced impact on PZT ferroelectric properties [3–5], which is microscopically attributed to the creation of charge compensating oxygen vacancies ($V_O^{\bullet\bullet}$). Recent EPR results on Fe^{3+}-doped '*hard*' PZT include the formation of a $(Fe'_{Zr,Ti} - V_O^{\bullet\bullet})^{\bullet}$ defect dipole for Fe^{3+}-doped PZT compounds [6–10]. On the other hand, the current understanding of acceptor doping also involves acceptor centers, such as Cr^{3+} [11] or Cu^{2+} in $PbTiO_3$ [9, 12, 13], where no defect association with charge compensating oxygen vacancies has yet been observed, such that rather 'isolated' defect centers are discussed being present.

A former X-band EPR investigation on Fe^{3+} impurity centers in nominally undoped PZT compounds reported the surprising observation that the Fe^{3+} center also probes rhombic symmetry in a range from PZT 10/90 to PZT 52/48, even though these PZT compositions are in the tetragonal region of the phase diagram [6], for which reason no rhombic symmetry is expected from the global crystal structure. In order to explain this discrepancy different models have been discussed including a segregation of the $(Fe'_{Zr,Ti} - V_O^{\bullet\bullet})^{\bullet}$ complex to grain boundaries; the existence of small non-tetragonal phases; a local clustering of zirconium ions; or the Fe^{3+} ion being surrounded by unit cells containing zirconium. Even though all of these models involve a symmetry-reduction

 © 2007 The Royal Swedish Academy of Sciences Printed in the UK

of the Fe^{3+}-site the underlying structural arrangement has remained an open question.

A point not yet exploited in the above discussed models is the defect chemistry by means of lattice vacancies. By invoking such defects, two more models emerge that explain a lower site symmetry. The first structural arrangement invokes a lead vacancy (V''_{Pb}) in the unit cell of the $(Fe'_{Zr,Ti} - V_O^{\bullet\bullet})^{\bullet}$ center. The second model is based on the fact that the $(Fe'_{Zr,Ti} - V_O^{\bullet\bullet})^{\bullet}$ defect dipole only conserves the tetragonal point symmetry at the iron site if the dipole is oriented along the crystallographic *c*-axis as has been found for Fe^{3+}-doped $PbTiO_3$ [7–9]. For an orientation of the $(Fe'_{Zr,Ti} - V_O^{\bullet\bullet})^{\bullet}$ defect dipole along the crystallographic *a*- and *b*-axes, analogous to Fe^{3+}-modified $PbZrO_3$ [9, 10] compounds, the local symmetry would also be reduced.

Furthermore, the current understanding of charge compensation for codoped '*soft*' piezoelectric compounds is that the creation of lead vacancies due to donor doping compensates the creation of oxygen vacancies by the simultaneous doping with acceptor ions. For the here studied (La^{3+}, Fe^{3+})-codoped PZT 40/60 material, the question thus arises if there is partial charge compensation of the acceptor-type $Fe'_{Zr,Ti}$ center by means of an associated $V_O^{\bullet\bullet}$ or if the charge is compensated exclusively accomplished by means of the donor-type $La^{\bullet}_{Pb}$ centers and additionally V''_{Pb}.

In order to discuss the above mentioned questions a multi-frequency EPR study of the Fe^{3+} functional center in (La^{3+}, Fe^{3+})-codoped $Pb[Zr_{0.4}Ti_{0.6}]O_3$ ceramics has been performed. As the La^{3+} functional center is diamagnetic, exclusively signals from the high-spin paramagnetic Fe^{3+} ion may be observed by means of EPR. In particular, the electronic fine-structure (FS) interaction induced by the crystal field originating from the nearest-neighbor O^{2-} ions and possibly oxygen vacancies around the Fe^{3+} center is exploited as a sensitive probe of the local symmetry at the dopant site.

2. Experimental

2.1. Sample preparation and characterization

PZT 40/60 containing 1 mol.% La and 0.5 mol.% Fe was prepared by the mixed oxide route. Taking into account the formation of lead and oxygen vacancies caused by the La and Fe dopants [14, 15], the material was prepared according to the chemical composition $Pb_{0.985}La_{0.01}(Zr_{0.398}Ti_{0.597}Fe_{0.005})O_{2.9975}$. PbO (Tetranox, Liebau), ZrO_2 (CS02, SEPR) TiO_2 (Tronox, Kerr Mc Ghee), La_2O_3 (Merck) and Fe_2O_3 (Merck) were attrition milled at 1000 rpm for 3 h in isopropanol using a polyamide crucible, polyamide stirrer and yttria stabilized tetragonal zirconia (YTZ) milling balls (2 mm). The slurry was then dried in a rotation distiller and stored at 100 °C for 48 h. After sieving the powder mixture (160 μm mesh) it was calcinated at 850 °C for 2 h in a closed alumina crucible. The calcinated powders were then ball milled in a planetary mill at 200 rpm for 6 h in isopropanol to reduce the particle size, dried for 4 days and sieved (16 μm mesh) in order to obtain a powder suitable for the dry forming procedure. Cylindrical pellets of 4.25 g were first uniaxially pressed in 12 mm dyes and then cold isostatically pressed at 400 MPa. The pellets were stored for several days at 100 °C under vacuum. Sintering at 1050 °C for 6 hours in air resulted in ceramics with a density of 7.78 g cm^{-3}. Mass losses during sintering were at 0.2 wt.% approximately.

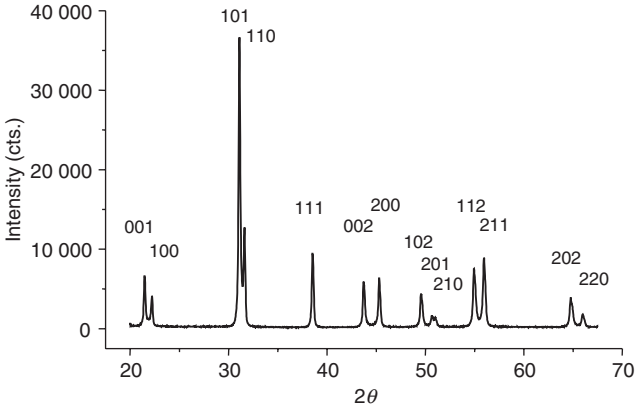

Figure 1. XRD pattern of PZT 40/60 codoped with 1.0 mol.% La^{3+}, and 0.5 mol.% Fe^{3+}.

From the sintered bodies slices were cut, ground and polished. Disk-shaped slices of 1 mm thickness were prepared for x-ray diffraction (XRD) experiments. These samples were heat treated for 4 h at 500 °C in order to reduce texture from the cutting and grinding procedures. Samples for the EPR measurements were fabricated by grinding and polishing slices to a thickness of 250 μm. Rectangular plates of 6×6 and $4 \times 6\,mm^2$ were machined from these thin slices. The former were used in the W-band experiments, the latter geometry was prepared for the X- and Q-band measurements.

XRD patterns were recorded in a Siemens D500 diffractometer with Cu K_α-radiation ($\lambda = 1.5406$ nm) equipped with a graphite secondary monochromator. The measurement covered an angular range between $2\Theta = 20.00°$ and 67.50° with a step size of 0.02°. Preliminary quantitative evaluation of the data focused on the {200} and {002} reflections, using Gauss–Lorentz profiles when fitting the peaks. The diffraction patterns of the ceramics show tetragonal phase as expected for the PZT 40/60 composition (figure 1). No indications for the presence of other phases can be found in the patterns. There is pronounced splitting between the {002} and {200} peaks. The lattice parameters as estimated from these peaks are $c = 4.136$ and $a = 3.999$, approximately. This corresponds to a lattice distortion $(c/a - 1)$ of 3.4%.

The intensity ratio I_{002}/I_{200} amounts to 0.92. The discrepancy with the theoretical value of 0.5, may be explained by a statistical distribution of domains, and indicates the presence of a surface texture from mechanical treatment that was not removed by the heat treatment. For tetragonal materials with high c/a-ratio, grinding typically induces textures which persist even after annealing above T_C, which recently has been observed for acceptor-, donor- and undoped PZT compounds [16]. The presence of surface texture therefore is not related to a particular type of dopant. The quantitative extent of texture, however, may be affected by dipole moments resulting from point defects or point defect associates [16].

2.2. Spectroscopic measurements

Multi-frequency-EPR was performed at three different Larmor frequencies. X-band (9.4 GHz) and Q-band (34 GHz) continuous wave EPR measurements were performed using a Bruker ESP 300E spectrometer with rectangular TE_{112} and dielectric cylindrical TE_{102} resonators, respectively. The magnetic field was read out with a NMR gaussmeter (ER 035M, Bruker). Cryogenic temperatures down to 10 K were provided by a helium-flow cryostat (Oxford). The applied microwave (mw) power was 1.0×10^{-3} mW and the field was modulated with a frequency of 100 kHz and amplitude of 0.1 mT. For the calibration of the resonance magnetic field values, a standard field marker (polycrystalline DPPH with $g = 2.0036$) was used. Field-modulated continuous wave EPR experiments at W-band (107.2 GHz) were performed at the National High Magnetic Field Laboratory (NHMFL) in Tallahassee, using a quartz synthesizer for the mw radiation in a set-up without resonator [17].

3. Theoretical description

The free trivalent iron ion, Fe^{3+}, possesses five unpaired electrons in the 3d shell ($3d^5$), resulting in an electronic $^6S_{5/2}$ ground state. The corresponding spin-Hamiltonian for this ion may be written as

$$\mathcal{H} = g_e \beta_e \mathbf{B_0} \cdot \mathbf{S} + \sum_{k=2,\ldots,5}^{-k \leqslant q \leqslant k} B_k^q \, O_k^q(S_x, S_y, S_z), \qquad (1)$$

in which the g-matrix is taken as isotropic with $g_e = 2.0023$, β_e denotes the Bohr magneton, $\mathbf{B_0}$ the external magnetic field, B_k^q are the FS spin-Hamiltonian parameters, and O_k^q are the extended Stevens spin operators [18, 19]. In principle all conceivable B_k^q parameters, resulting from 2nd-, 3rd-, 4th- and 5th-rank tensors, have to be considered [20]. However, all $B_{k>2}^q$ parameters for Fe^{3+} are orders of magnitude smaller than the dominant B_2^q terms and could not be detected in our spectra.

The spin-Hamiltonian parameters given in equation (1) are subject to numerical spectrum simulation and provide a basis for interpreting the structural characteristics at the Fe^{3+} functional center site.

4. Results

For X-band frequencies (9.4 GHz), the FS interaction of the Fe^{3+} functional center is considerably larger than the applied mw energy quanta ($3B_2^q \gg h\nu_{\mathrm{mw}}$). In this so-termed *low-frequency regime*, the EPR spectrum mainly consists of two prominent features at low fields as depicted in figure 2(a). In this situation, information may only be obtained regarding the local site symmetry of the Fe^{3+} functional center. On the other hand, size and sign of the Fe^{3+} FS parameters are not accessible. The obtained spectrum is similar to the ones obtained for Fe^{3+} defect centers in nominally undoped PZT [6]. Their origin is indicative of a situation in which the Fe^{3+} ion probes different distortions of the surrounding oxygen octahedron. Typically, these deviations from ideal octahedral symmetry are caused by oxygen vacancies. Here,

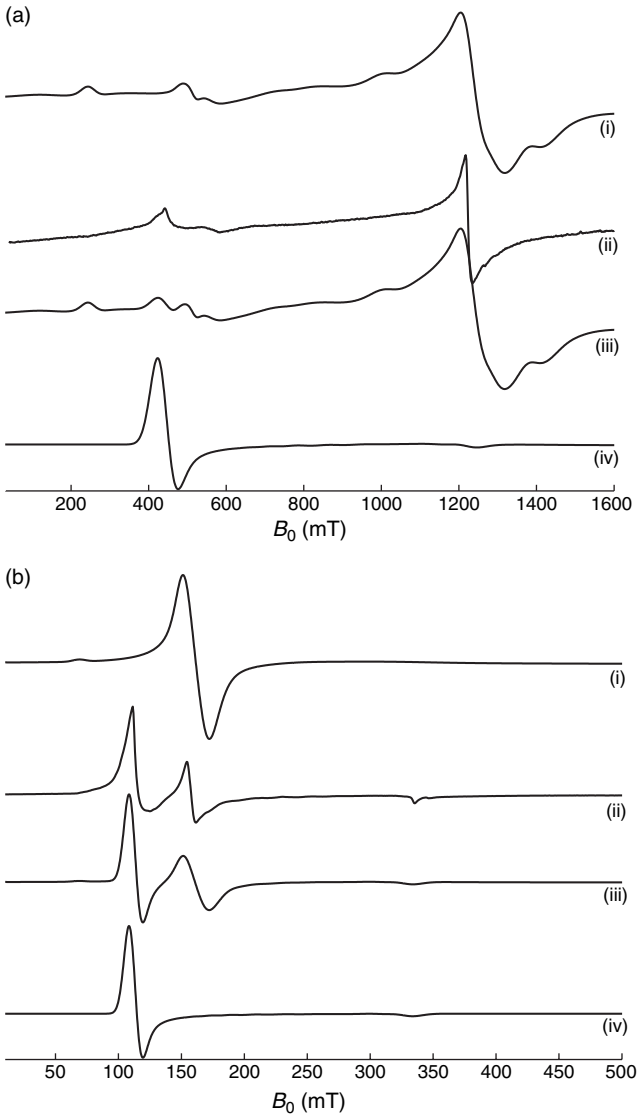

Figure 2. X- (a) and Q-band (b) EPR spectra at 10 K of PZT 40/60 codoped with 1.0 mol.% La^{3+} and 0.5 mol. % Fe^{3+}. (ii) Experimental spectra. (i) and (iv) Numerically simulated spectra of the purely 'tetragonal' and 'rhombic' phases. (iii) Numerically simulated sum spectra.

two spectroscopically superimposed centers are observed that reveal 'tetragonal' and 'rhombic' site symmetry, respectively. In order to analyze the Fe^{3+} FS interaction in more detail, high Larmor frequencies have to be used.

The advantage of a multi-frequency EPR analysis is that the used Larmor frequencies may selectively be chosen in order to spectroscopically separate overlapping features provided the intrinsic FS parameters for the two different centers significantly differ in magnitude. Obviously, in this case at Q-band frequencies (34 GHz), the 'tetragonal' center remains in the low-frequency regime, whereas for the 'rhombic' center an *intermediate-frequency regime* ($3B_2^q \approx h\nu_{\mathrm{mw}}$) is established, allowing for a determination of the corresponding $B_2^{0,2}$ FS parameters for the 'rhombic' center. The corresponding EPR spectrum is represented in figure 2(b).

On the other hand, by using even higher Larmor frequencies, at W-band (107 GHz) for the 'rhombic' center the *high-frequency regime* ($h\nu_{mw} \gg 3B_2^q$) is established.

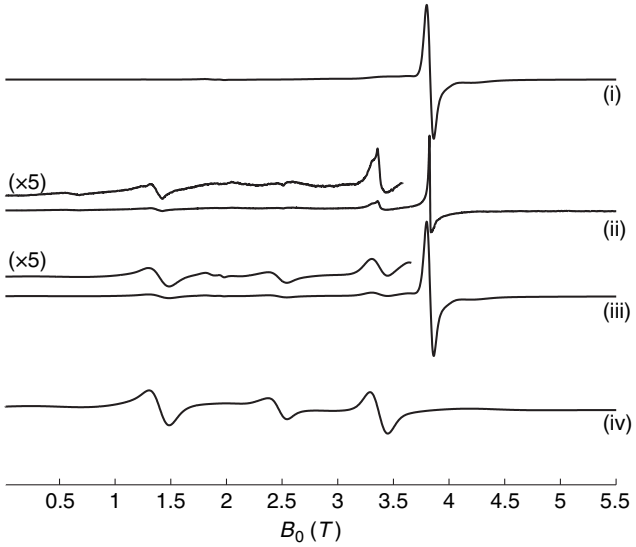

Figure 3. W-band EPR spectrum at 10 K of PZT 40/60 codoped with 1.0 mol.% La^{3+} and 0.5 mol.% Fe^{3+}. (ii) Experimental spectrum. (i) and (iv) Numerically simulated spectra of the purely 'tetragonal' and 'rhombic' phases. (iii) Numerically simulated sum spectrum.

Table 1. Spin-Hamiltonian parameters for the 'rhombic' and 'tetragonal' centers at 10 K in PZT 40/60 codoped with 1.0 mol.% La^{3+}, 0.5 mol.% Fe^{3+}, as obtained by the multifrequency numerical spectrum simulation.

	g_{iso}	B_2^0 (GHz)	B_2^2 (GHz)
'Rhombic' center	2.002	2.1(5)	0.7(5)
'Tetragonal' center	2.002	12.2(5)	–

In contrast, the 'tetragonal' center now is in an intermediate-frequency regime, allowing for a determination of the corresponding B_2^0 FS parameter for the 'tetragonal' center. The corresponding EPR spectrum is shown in figure 3.

The intermediate-frequency regime-type EPR spectra are typically represented by multiple resonance lines spanned over a wide magnetic field range. These include the so-called 'looping transitions' that do not continue over all possible orientations, and 'crossing transitions' that degenerate at specific orientations [21]. The resulting spectra are complicated and, consequently, for an accurate determination of FS parameters a refinement of the spin-Hamiltonian parameters through numerical spectrum simulation simultaneously for all used mw frequencies is needed. The corresponding results are summarized in table 1. Using these best-fit values, numerically simulated spectra are superimposed onto the experimental data and show good agreement. Furthermore, from the numerical simulation, the relative intensity ratio of 'tetragonal' and 'rhombic' centers may be extracted. For the here studied (La^{3+}, Fe^{3+})-modified PZT 40/60, we find a tetragonal-to-rhombic ratio of 1.7(2) at 10 K.

5. Discussion

Considering the refined Fe^{3+} FS values, the conclusion may be drawn that the iron functional center builds a charged defect associated with a directly coordinated oxygen vacancy, $(Fe'_{Zr,Ti} - V_O^{\bullet\bullet})^{\bullet}$, also for '*soft*' compounds in analogy to (La,Fe)-codoped PZT 52.5/47.5, where the observed Fe^{3+} FS parameters are of similar magnitude [14]. Concerning the charge compensation mechanism for the aliovalent La^{3+} and Fe^{3+} centers, a situation is present where partial charge compensation is accomplished by the fact that the Fe^{3+} builds a defect associated with an oxygen vacancy in the first coordination sphere. Global electro-neutrality is achieved based on the creation of additional lead vacancies, as no additional valency-altered centers such as Ti^{3+}, Zr^{3+}, Pb^{+} or Pb^{3+} and no e' or $h^{\bullet}$ centers, all of which are paramagnetic, have been observed in this study. This observation supports the findings for the pure-member systems of '*hard*' Fe^{3+}-modified $PbTiO_3$ [7, 8] and $PbZrO_3$ [10], as well as '*soft*' Gd^{3+}-doped $PbTiO_3$ [22]. The two assumptions that donor-doping tends to result in components with vanishing $V_O^{\bullet\bullet}$-content and that internal bias fields by means of $(Fe'_{Zr,Ti} - V_O^{\bullet\bullet})^{\bullet}$-type defect dipoles, are only present in acceptor-doped '*hard*' compounds may thus not be upheld for the here studied (La^{3+}, Fe^{3+})-modified PZT 40/60 ceramics.

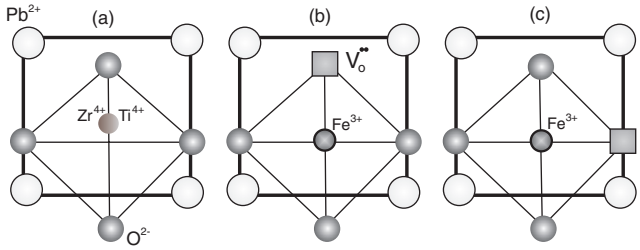

Figure 4. Schematic representation of the proposed structural models. (a) Unit cell of the undoped compound. (b) 'Tetragonal' center. (c) 'Rhombic' center.

The most important structural feature emerging from the evaluation of the EPR spectra is that the 'truncated' oxygen octahedra that surround the Fe^{3+} dopant ions are not homogeneously tetragonally distorted, as is the case for the octahedra in unit cells containing Zr^{4+} or Ti^{4+}, but also exhibit a fraction of rhombohedrally distorted ones. From the tetragonal crystal structure a tetragonal distortion can be expected, the amount of distortion is however considerably different from the effects that could result from the shifts in oxygen ions due to the tetragonality of the unit cells. A rhombohedral distortion cannot be explained from global crystal symmetry of the material at all. Therefore, it is concluded, that local properties in the environment of the Fe^{3+} dopant ions are the physical origin of the distortion. It is suggested that all dopant Fe^{3+} ions are associated with oxygen vacancies $V_O^{\bullet\bullet}$, located in the first coordination sphere of the Fe^{3+}. Exploiting the existence of the $(Fe'_{Zr,Ti} - V_O^{\bullet\bullet})^{\bullet}$ defect dipole, the two observed centers of different site symmetry may be explained by means of their relative orientation with respect to the direction of spontaneous polarization. The 'tetragonal' center conserves the tetragonal point symmetry at the iron site owing to an orientation along the crystallographic *c*-axis. On the other hand, the 'rhombic' center is due to an orientation of the $(Fe'_{Zr,Ti} - V_O^{\bullet\bullet})^{\bullet}$ defect dipole along the crystallographic *a*- and *b*-axes, which reduces the iron-site symmetry. The corresponding structural arrangement is schematically illustrated in figure 4.

Acknowledgments

This research has been financially supported by the DFG centre of excellence 595 '*Electrical Fatigue in Functional Materials*'. Fruitful discussions, continuous support and the use of an X-band EPR spectrometer in the laboratory of Professor Dr K-P Dinse is gratefully acknowledged. We thank Dr Yan Xin for the valuable technical support in machining the samples at the NHMFL.

References

[1] Hoffmann M J and Kungl H 2004 *Curr. Opin. Solid State Mater. Sci.* **8** 51–7
[2] Eichel R-A 2007 *J. Electroceram.* **19** 9–21
[3] Hennings D and Pomplun H 1974 *J. Am. Ceram. Soc.* **57** 527
[4] Takahashi S 1982 *Ferroelectrics* **41** 143
[5] Smyth D M 1991 *Ferroelectrics* **116** 117
[6] Warren W L, Tuttle B A, Rong F C, Gerardi G J and Poindexter E H 1997 *J. Am. Ceram. Soc.* **80** 680–4
[7] Meštrić H, Eichel R-A, Dinse K-P, Ozarowski A, van Tol J and Brunel L C 2004 *J. Appl. Phys.* **96** 7440–4
[8] Meštrić H, Eichel R-A, Kloss T, Dinse K-P, Laubach So, Laubach St and Schmidt P C 2005 *Phys. Rev.* B **71** 134109
[9] Eichel R-A, Meštrić H, Dinse K-P, Ozarowski A, van Tol J, Brunel L C, Kungl H and Hoffmann M J 2005 *Magn. Reson. Chem.* **43** S166–76
[10] Meštrić H *et al* 2006 *Phys. Rev.* B **73** 184105
[11] Erdem E, Böttcher R, Semmelhack H C, Gläsel H J and Hartmann E 2003 *Phys. Status Solidi b* **239** R7–9
[12] Eichel R-A, Kungl H and Hoffmann M J 2007 *J. Appl. Phys.* **95** 8092–6
[13] Eichel R-A, Dinse K-P, Kungl H, Hoffmann M J, Ozarowski A, van Tol J and Brunel L C 2005 *Appl. Phys.* A **80** 51–4
[14] Erdem E, Eichel R-A, Kungl H, Hoffmann M J, Ozarowski A, van Tol H and Brunel L C 2007 *IEEE Trans. UFFC* at press
[15] Jaffe B, Cook W R and Jaffe H 1971 *Piezoelectric Ceramics* (London: Academic)
[16] Hammer M, Monty C, Endriss A and Hoffmann M J 1998 *J. Am. Cer. Soc.* **81** 721–4
[17] van Tol J, Brunel L C and Wylde R J 2005 *Rev. Sci. Instrum.* **76** 074101
[18] Abragam A and Bleaney B 1970 *Electron Paramagnetic Resonance of Transition Ions* (Oxford: Clarendon)
[19] Rudowicz C 1987 *Magn. Reson. Rev.* **13** 1–89
[20] Grachev V G 1987 *Sov. Phys.—JETP* **65** 1029–35
[21] Misra K S 1999 *J. Magn. Res.* **137** 83–92
[22] Eichel R-A, Meštrić H, Kungl H and Hoffmann M J 2006 *Appl. Phys. Lett.* **88** 122506